Research Square

Preprints are preliminary reports that have not undergone peer review.
They should not be considered conclusive, used to inform clinical practice,
or referenced by the media as validated information.

Microscopic to macroscopic models of the optimal velocity model for pedestrian evacuation during the dispersion of smoke

Juntima Makmul

fscijtm@ku.ac.th

Kasetsart University

Research Article

Keywords: Microscopic optimal velocity model, Pedestrian evacuation model, Smoke dispersion, Macroscopic pedestrian models, Particle method

Posted Date: May 29th, 2026

DOI: https://doi.org/10.21203/rs.3.rs-9776335/v1

License: This work is licensed under a Creative Commons Attribution 4.0 International License.
Read Full License

Additional Declarations: No competing interests reported.

Microscopic to macroscopic models of the optimal velocity model for pedestrian evacuation during the dispersion of smoke

J. Makmul*

May 21, 2026

Abstract

The microscopic optimal velocity model is applied to simulate movements of pedestrians. It is extended by coupling with the advection-diffusion equation and the Eikonal equation. The advection-diffusion equation is used for smoke propagation and the Eikonal equation is employed for guiding moving directions of pedestrians. These together are applied for simulations of pedestrians during smoke spreading. The derivations starting from the scaled microscopic optimal velocity model for particles' distributions during the dispersion of smoke to the corresponding mean field equation, hydrodynamic and scalar models are demonstrated. Several numerical experiments are investigated and results are compared. The advantage of using macroscopic models over the microscopic model is described.

Keywords: Microscopic optimal velocity model; Pedestrian evacuation model; Smoke dispersion; Macroscopic pedestrian models; Particle method.

1 Introduction

Numerous pedestrian models used to study pedestrian movements exist in many fields of study. It ranges from microscopic, mesoscopic and macroscopic models. For microscopic model, it takes into account pedestrian characteristics such as individual desired movement direction, the interactions between particles or individual desired speed. Examples for pedestrian microscopic models are cellular automata model [1], social force model [2,3], optimal velocity model [4], magnetic force model [5] or discrete choice model [6]. For mesoscopic model or kinetic model, it considers groups or distributions of particles. The state of this system is introduced by an appropriate probability distribution over the particle interactions of microscopic state. Examples of mesoscopic models for

*Kasetsart University, Department of Mathematics, Science Faculty, Thailand (fscijtm@ku.ac.th).

crowds are presented in references [7]. Macroscopic pedestrian models represent crowds as continuous medium using average quantities such as density, average velocity or energy. Examples of first order macroscopic model or scalar model is reference [8] and second order macroscopic model is reference [9].

In this research, we consider the microscopic optimal velocity model for pedestrian crowd [10] and extend it by coupling the advection-diffusion equation applied for the dispersion of smoke. This is used for simulating movements of pedestrians during propagation of smoke. The Eikonal equation [11] is also coupled to the microscopic optimal velocity model for guiding movement directions of particles, which depends on pedestrian density as well as on smoke density. This setting navigates pedestrians to move towards the destination simultaneously avoiding areas with high pedestrian and smoke density.

Then we show the derivation of the corresponding mean field equation, hydrodynamic model and scalar model to the scaled microscopic optimal velocity model. For hydrodynamic and scalar models, we consider them in a Lagrangian descriptions and obtain system of ODE equations. These ODE equations of microscopic and macroscopic models are solved by the explicit Euler method. The advection-diffusion equation for spreading of smoke is approximated by the operator splitting method. To solve the Eikonal equation, the fast marching method [12] is employed.

Several numerical experiments are conducted and the results are analyzed. For similar derivations from the scaled microscopic model to the corresponding mean filed equation, hydrodynamic model and scalar model, we refer to reference [13] for pedestrian flow based on the social force model with optimal path, in the reference [14] for the case of swarming model and in the reference [15] for complex material flow problem.

This article is organized as follows. We present the microscopic optimal velocity model coupled with the advection-diffusion equation and the Eikonal equation using for simulating pedestrian movements during propagation of smoke. The corresponding mean field equation, hydrodynamic and scalar models are demonstrated in Section 2. Numerical methods use for approximating the solutions of ODE system, the advection-diffusion equation and the Eikonal equation are described in Section 3. In section 4, we display results of numerical experiments. Finally, conclusions are proposed in section 5.

2 The Models

In this section, we introduce the microscopic optimal velocity model to simulate pedestrians' movements during the propagation of smoke. We explain the way to couple the advection-diffusion equation applied for smoke density to the microscopic optimal velocity model. The movement direction of a pedestrian is determined by the solution of the Eikonal equation, which depends on pedestrian density as well as on smoke density. This would lead pedestrian to move towards destination as well as on avoiding areas with high pedestrian and smoke density. Then we present the derivations of the corresponding mean filed equation, hydrodynamic model and scalar model to the microscopic optimal velocity model.

2.1 Microscopic Optimal Velocity Model

The microscopic optimal velocity model for pedestrians' movements is described by the ODE system as following [10]

$$\frac{dx_i}{dt} = v_i, \tag{2.1}$$

$$\frac{dv_i}{dt} = a(v^0 - v_i) + \sum_{i \neq j} H(x_i, x_j),\ i = 1, 2, ..., N, \tag{2.2}$$

where $x_i,\ v_i \in \mathbb{R}^2$ are position and actual velocity of pedestrian i, respectively. N be the total number of pedestrians in simulation. The term $a(v^0 - v_i)$ refers to the desire force, where a is a sensitive parameter. v^0 gives the direction to the destination that depends on pedestrian density likewise on smoke density. It describes as follows

$$v^0 = U_{max}\Big(1 - \frac{\rho(x,t)}{\rho_{max}}\Big)\nu(x_i), \tag{2.3}$$

where U_{max} and ρ_{max} are maximum speed and density of pedestrian, respectively. $\rho(x,t)$ is pedestrian density at point x in time t. $\nu(x_i)$ is the unit vector pointing in the direction to destination that avoids areas with high pedestrian density, high smoke density and obstacles. It is expressed as follows

$$\nu(x_i) = -\frac{\nabla T(x_i)}{|\nabla T(x_i)|}, \tag{2.4}$$

where T is the solution of the Eikonal equation [12]

$$|\nabla T(x)| = \frac{1}{F(x)}, \quad x \in \Omega. \tag{2.5}$$

Ω is a simulation domain. $T(x)$ is the arrival time to reach the destination at point x. It is set to zero for destination areas. The moving speed of the front

$F(x) > 0$ is assigned to

$$F(x) = \begin{cases} 0.01 & , \quad x \in \Omega_b \\ U_{max}\Big(1 - \dfrac{\rho(x,t)}{\rho_{max}}\Big) & , \quad x \in \Omega/\Omega_b. \end{cases} \tag{2.6}$$

Ω_b is obstacle or high smoke density regions. A low value of $F(x)$ is set in obstacle and high pedestrian density areas. This yields a large value of arrival time $T(x)$ in equation (2.5). Therefore, pedestrians will not move into these zones. $F(x)$ is set to $U_{max}\Big(1 - \dfrac{\rho(x,t)}{\rho_{max}}\Big)$ in areas without obstacle. This moving speed of the front $F(x)$ relies on pedestrian density $\rho(x,t)$. When pedestrian density $\rho(x,t)$ reaches ρ_{max}, a low value of the front speed $F(x)$ is attained that leads to large arrival time $T(x)$. Pedestrians reject to move to this point.

The interaction force between particles displayed by the term $H(x_j - x_i)$ in equation (2.2) is given by

$$H(x_i, x_j) = \alpha[\tanh\beta(d_{ji} - b) + c](1 + \cos\varphi)n_{ji} \tag{2.7}$$

with

$$\cos\varphi = \frac{x_j^{(1)} - x_i^{(1)}}{d_{ji}}, \tag{2.8}$$

where α, β, b and c are parameters. $d_{ji} = |x_j - x_i|$ is the distance between pedestrians i-th and j-th. The normalized vector pointing from pedestrian i to pedestrian j is represented as $n_{ji} = \dfrac{x_j - x_i}{d_{ji}}$. φ is the angle between $x_j - x_i$ and the moving direction v^0. The term $(1 + \cos\varphi)$ shows the anisotropic behavior that pedestrian responses to the situation in front of him stronger than the situation behind him.

The dispersion of smoke and smoke density in simulation domain is received by solving the following linear advection-diffusion equation [1]

$$\frac{\partial C}{\partial t} + w \cdot \nabla C = \kappa_d \nabla^2 C + S(x_s, t) \in \Omega \times \mathbb{R}^+ \tag{2.9}$$

with the Dirichlet boundary conditions where $C(x,t) = 0$ on the boundary of domain. $C(x,t)$ is smoke density at position x at time t and $\Omega \subset \mathbb{R}^2$ is the simulation domain. $w = (w_1, w_2) \in \mathbb{R}^2$ is the smoke velocity field showing the spreading direction of smoke. $\kappa_d > 0$ is the diffusion constant and $S(x_s, t)$ is the smoke source at point x_s. The smoke concentration threshold $C(x) \geq 0.05$ is assumed to be high smoke density. This value reduces the visibility range of a pedestrian to about 6 m - 7 m that effects pedestrian speed significantly as reported in [1,16,17].

2.2 Mean field equation

The procedure to obtain the corresponding mean field equation to the microscopic model for large number of particles is conducted in a similar way as in the reference [14]. The difference between our model to the reference [14] is the scaled microscopic model inserted to the Liouville equation. In the reference [14] it is for swarm model and our scaled microscopic model is for pedestrian movement based on the optimal velocity model. To attain the mean field equation, we start with the Liouville equation

$$\frac{\partial f^{(N)}}{\partial t} + \sum_{i=1}^{N} \Big[\mathrm{div}_{x_i} \Big(\frac{dx_i}{dt} f^{(N)} \Big) + \mathrm{div}_{v_i} \Big(\frac{dv_i}{dt} f^{(N)} \Big) \Big] = 0, \tag{2.10}$$

where $f^{(N)} = f^{(N)}(x_1, ..., x_N, v_1, ..., v_N)$ be the N-particle probability density function. The terms $\dfrac{dx_i}{dt}$ and $\dfrac{dv_i}{dt}$ are the microscopic optimal velocity model for pedestrians with the interaction force $H(x_i, x_j)$ scaled by a factor $\dfrac{1}{N}$ using the *weak coupling scaling* hereinafter

$$\frac{dx_i}{dt} = v_i, \tag{2.11}$$

$$\frac{dv_i}{dt} = a(v^0 - v_i) + \frac{1}{N} \sum_{i \neq j} H(x_i, x_j), \ i = 1, 2, ..., N. \tag{2.12}$$

The one particle distribution function $f^{(1)}$ is defined as

$$f^{(1)}(x_1, v_1) = \int f^{(N)} d\Omega_1,$$

where $d\Omega_1 = dx_2 ... dx_N dv_2 ... dv_N$. Then we integrate the Liouville equation (2.10) over $d\Omega_1$

$$\int \frac{\partial f^{(N)}}{\partial t} d\Omega_1 + \int \mathrm{div}_{x_1} \Big(\frac{dx_1}{dt} f^{(N)} \Big) d\Omega_1 + \int \mathrm{div}_{v_1} \Big(\frac{dv_1}{dt} f^{(N)} \Big) d\Omega_1 = 0. \tag{2.13}$$

Replacing $\dfrac{dx_1}{dt} = v_1$ and $\dfrac{dv_1}{dt} = a(v^0 - v_1) + \dfrac{1}{N} \sum_{j \neq 1} H(x_1, x_j)$ in equation (2.13) and restricting to the case of $f^{(1)}$. Equation (2.13) turns into

$$\frac{\partial f^{(1)}}{\partial t} + v_1 \cdot \nabla_{x_1} f^{(1)} + \mathrm{div}_{v_1} [a(v^0 - v_1) f^{(1)}] + \mathrm{div}_{v_1} \int \frac{1}{N} \sum_{j \neq 1} H(x_1, x_j) f^{(N)} d\Omega_1 = 0. \tag{2.14}$$

Considering the last term of equation (2.14), we obtain the following equation by the assumption of indistinguishable particles.

$$\frac{N-1}{N} \mathrm{div}_{v_1} \int H(x_1, x_2) f^{(2)} dx_2 dv_2, \tag{2.15}$$

where

$$f^{(2)}(x_1, x_2, v_1, v_2) = \int f^{(N)} dx_3 ... dx_N dv_3 ... dv_N,$$

$f^{(2)}(x_1, x_2, v_1, v_2)$ is the two particle probability function. After that we assume the factorization of $f^{(2)}$, i.e. $f^{(2)}(x_1, x_2, v_1, v_2) = f^{(1)}(x_1, v_1) f^{(1)}(x_2, v_2)$. Hence equation (2.15) becomes

$$\frac{N-1}{N} \mathrm{div}_{v_1} \int H(x_1, x_2) f^{(1)}(x_2, v_2) f^{(1)}(x_1, v_1) dx_2 dv_2. \tag{2.16}$$

Due to $\rho(x,t) = \int f(x, v, t) dv$, equation (2.16) can be written as

$$\frac{N-1}{N} \mathrm{div}_{v_1} \int H(x_1, x_2) \rho(x_2, t) f^{(1)}(x_1, v_1) dx_2. \tag{2.17}$$

We substitute the last term of equation (2.14) with equation (2.17). Equation (2.14) becomes

$$\frac{\partial f^{(1)}(x_1, v_1)}{\partial t} + v_1 \cdot \nabla_{x_1} f^{(1)} + \mathrm{div}_{v_1}[a(v^0 - v_1) f^{(1)}] + \frac{N-1}{N} \mathrm{div}_{v_1} \int H(x_1, x_2) \rho(x_2, t) f^{(1)}(x_1, v_1) dx_2 = 0. \tag{2.18}$$

Replacing $f^{(1)}(x_1, v_1)$ with $f(x, v, t)$ and taking the limit $N \to \infty$, finally we achieve the mean field equation

$$\frac{\partial f}{\partial t} + v \cdot \nabla_x f + \mathrm{div}_v[a(v^0 - v) f] + \mathrm{div}_v \int H(x, y) \rho(y, t) f dy = 0. \tag{2.19}$$

2.3 Hydrodynamic model

To attain the corresponding hydrodynamic model to the scaled microscopic optimal velocity model (2.11-2.12), we proceed similar way as in reference [18]. Starting from the mean field equation (2.19), we integrate equation (2.19) against v and vdv. The fluctuation terms are neglected, i.e. the velocity distribution is monokinetic: $f(x, v, t) = \rho(x, t)\delta(v - u(x, t))$, where δ is the Dirac delta function, we obtain the following hydrodynamic model

$$\frac{\partial \rho}{\partial t} + \nabla_x \cdot (\rho u) = 0, \tag{2.20}$$

$$\frac{\partial u}{\partial t} + (u \cdot \nabla_x) u = a(v^0 - u) + \int H(x, y) \rho(y) dy. \tag{2.21}$$

The elaborate details for deriving similar macroscopic system, we refer to references [13,18]. Similar hydrodynamic models can be found in reference [14] for swarm model, in reference [15] for complex material flow problems and in references for pedestrian flow based on the social force model [11,13].

2.4 The Scalar Model

To obtain the scalar model, we start with the hydrodynamic momentum equation (2.21). Neglecting the inertial effects and the time change terms, we get

$$a(v^0 - u) = -\int H(x,y)\rho(y)dy. \tag{2.22}$$

Solving equation (2.22) for u provides us

$$u = v^0 + \frac{1}{a}\int H(x,y)\rho(y)dy.$$

This u is applied in the continuity equation (2.20) and it gives us the following scalar equation

$$\frac{\partial \rho}{\partial t} + \nabla_x \cdot (\rho(v^0 + \frac{1}{a}\int H(x,y)\rho(y)dy)) = 0. \tag{2.23}$$

3 Numerical Methods

In this section, we describe numerical methods to approximate solutions of the microscopic optimal velocity model (2.1-2.2) and (2.11-2.12), hydrodynamic model (2.20-2.21), scalar model (2.23), the Eikonal equation (2.5) and the advection-diffusion equation (2.9).

3.1 Microscopic optimal velocity simulation

The simulation domain of the microscopic optimal velocity model is discretized into rectangular cells of size 0.5 m $\times$ 0.5 m. The local particle density of each cell is calculated by following

$$\rho = \frac{N_t}{N_{max}},$$

where N_t is the number of actual particles in the cell at time t and N_{max} is the maximum number of pedestrians in one cell generated at initial time. The average velocity u of each cell is computed by averaging the pedestrian velocities lied in that cell. The ODE systems of the microscopic optimal velocity model (2.1-2.2) and (2.11-2.12) for the scaled one are solved numerically by the explicit Euler method with time step 0.02.

3.2 Macroscopic simulations

For macroscopic simulations, we consider in a Lagrangian descriptions. Thus the hydrodynamic equations (2.20-2.21) in a Lagrangian formulation read as

$$\frac{dx}{dt} = u, \tag{3.1}$$

$$\frac{d\rho}{dt} = -\rho\frac{\partial u}{\partial x}, \tag{3.2}$$

$$\frac{du}{dt} = a(v^0 - u) + \int H(x,y)\rho(y)dy, \tag{3.3}$$

where $\dfrac{d}{dt} = \partial_t + u \cdot \nabla_x$. We evaluate these quantities at the particle location and approximate the spatial derivative of u by a corrective smoothed particle method (CSPM) [19].

$$\frac{\partial u_i}{\partial x_i} = \frac{\sum_{j=1}^{N_b} \frac{m_j}{\rho_j}(u_j - u_i)\frac{\partial W_{ij}}{\partial x_i}}{\sum_{j=1}^{N_b} \frac{m_j}{\rho_j}(x_j - x_i)\frac{\partial W_{ij}}{\partial x_i}}, \tag{3.4}$$

where $u_i = u(x_i) \in \mathbb{R}^2$ and $x_i \in \mathbb{R}^2$. $W_{ij} = W(x_i - x_j, h)$ is the smoothing function whose support domain is defined by the smoothing length h. N_b is the number of particles in the support domain. m_j and ρ_j are the mass and density of particle j. The following cubic spline function is applied as the smoothing function [20]

$$W_{ij} = \frac{15}{7\pi h^2}\begin{cases} \dfrac{2}{3} - \vartheta^2 + \dfrac{1}{2}\vartheta^3 & , \quad 0 \le \vartheta < 1, \\ \dfrac{1}{6}(2-\vartheta)^3 & , \quad 1 \le \vartheta < 2, \\ 0 & , \quad \vartheta \ge 2, \end{cases} \tag{3.5}$$

where $\vartheta = \dfrac{|x_i - x_j|}{h}$. The integral over the interaction force is computed by a straight-forward integration rule, i.e.,

$$\int H(x,y)\rho(y)dy \sim \sum_j H(x,x_j)\rho_j dV_j, \tag{3.6}$$

where dV_j is the local area around particle j which is determined by a nearest neighbor search. Finally, the scalar model (2.23)

$$\frac{\partial \rho}{\partial t} + \nabla_x(b\rho) = 0,$$

with

$$b = v^0 + \frac{1}{a}\int H(x,y)\rho(y)dy,$$

it is considered as well in a Lagrangian description written below

$$\frac{dx}{dt} = b, \tag{3.7}$$

$$\frac{d\rho}{dt} = -\rho \frac{\partial b}{\partial x}. \tag{3.8}$$

The spatial derivative of b is approximated using the CSPM method as in the hydrodynamic model, i.e.,

$$\frac{\partial b_i}{\partial x_i} = \frac{\sum_{j=1}^{N_b} \frac{m_j}{\rho_j}(b_j - b_i)\frac{\partial W_{ij}}{\partial x_i}}{\sum_{j=1}^{N_b} \frac{m_j}{\rho_j}(x_j - x_i)\frac{\partial W_{ij}}{\partial x_i}}. \tag{3.9}$$

Particles in macroscopic simulations are placed at the cell center of microscopic cells at initial time and the ODE systems (3.1-3.3) and (3.7-3.8) are solved by the explicit Euler method with time step 0.02.

3.3 Solving the advection-diffusion equation

To solve the advection-diffusion equation, we generate the space grids of size 0.2 and time step is set to 0.02. The operator splitting method with Dirichlet boundary conditions are applied to approximate the solution of the advection-diffusion equation. This method splits into two parts over two time steps, i.e., it solves first in the x-direction and then the results are applied to solve in the y-direction separately. Details of this method, we refer to the reference [1].

3.4 Solving the Eikonal equation

The Eikonal equation is employed to guide moving directions of particles, which depends on pedestrian density as well as on smoke density. The same space grids as solving the advection-diffusion equation of size 0.2 is used to solve the Eikonal equation. Hence each grid point of the Eikonal equation, we obtain the information of smoke density that is used for setting in equation (2.6). The Eikonal equation is solved numerically by the well known fast marching method. This method constructs the solution outwards from the destination which ranges from smallest to largest arrival time. Details of this method are described in references [12].

4 Numerical Experiments and Results

We set the numerical experiments on the domain as in reference [11], which is a corridor of length 20 m and width of 10 m. There are two exits with size 2 m on the right side of the corridor, which is labeled with red color as in Figure 1. The blue rectangular on the left side of the corridor is the area where particles are generated at initial time. Cells of size 0.5 m $\times$ 0.5 m are generated on the simulation domain. The scaled microscopic optimal velocity model (2.11-2.12),

hydrodynamic model (2.20-2.21) and scalar model (2.23) are employed in our experiments. Time to simulate an experiment is set to 25 s. In the scenarios with smoke, we assume that smoke is emitted at the source point with constant rate 10 g/s in each time step. Parameters used for tests give as in Table 1. All programs are implemented with MATLAB on a HP Intel(R) Core(TM) i7-7700CPU, 3.6GHz computer. We perform several experiments as follows.

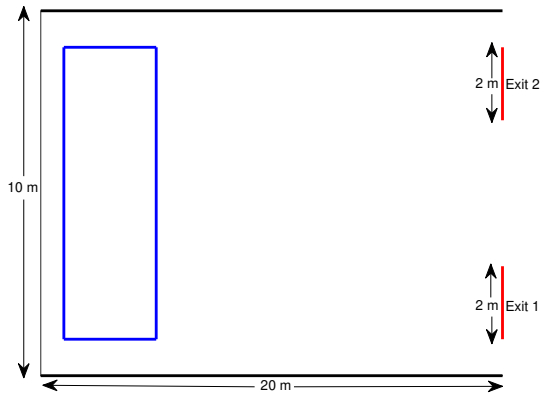


Figure 1: The modeling area for numerical experiments [11].

Parameters	Value			Equation
	micro	hydro	scalar	
a	1	1	1	(2.2), (2.21), (2.23), (3.3)
U^{max}	1	1	1	(2.3), (2.6)
ρ^{max}	10	10	10	(2.3), (2.6)
α	0.25	0.25	0.25	(2.7)
β	2.5	2.5	2.5	(2.7)
b	1	1	1	(2.7)
c	-1	-1	-1	(2.7)
w_1	[-0.5,0.5]	[-0.5,0.5]	[-0.5,0.5]	(2.9)
w_2	[-0.5,0.5]	[-0.5,0.5]	[-0.5,0.5]	(2.9)
κ_d	0.05	0.05	0.05	(2.9)
m_j	-	1	1	(3.4), (3.9)
h	-	0.8	0.8	(3.5)

Table 1: Parameters for microscopic, hydrodynamic and scalar simulations.

4.1 Experiment 1

In the first experiment, we compare numerical comparisons between situations with and without smoke of the scaled microscopic optimal velocity model (2.11-2.12), hydrodynamic model (2.20-2.21) and scalar model (2.23). For microscopic simulations, 5 particles are randomly distributed in each cell within blue rectangular area of the corridor at initial time. Therefore, there are 640 particles for microscopic simulation. For macroscopic simulations, a particle is placed in the middle of the cell within blue rectangular area of the corridor. Hence 120 particles is used for hydrodynamic and scalar models. A smoke source is placed at position $(8, 5)$ which is in the middle of corridor for smoke scenario. Figure 2 shows number of outside pedestrians of microscopic optimal velocity model in the case with and without smoke in simulations. It obviously see that number of outside pedestrians in the case without smoke is greater than situation with smoke. Pedestrians start to leave the corridor at time about 16 s. All pedestrians can evacuate out of corridor about 22 s in the case without smoke and about 25 s for smoke situation. Pedestrians need to avoid dense smoke areas that it leads to longer evacuation time in smoke case than situation without smoke. Figure 3 shows particles' distributions at time 10 s of the scaled microscopic, hydrodynamic and scalar models in situation with and without smoke. Hydrodynamic and scalar models provide similar results to scaled microscopic model both in case with and without smoke source in experiments. Particles are separated into two groups and moving towards the exits. In smoke scenarios, particles avoid moving into areas with high smoke density.

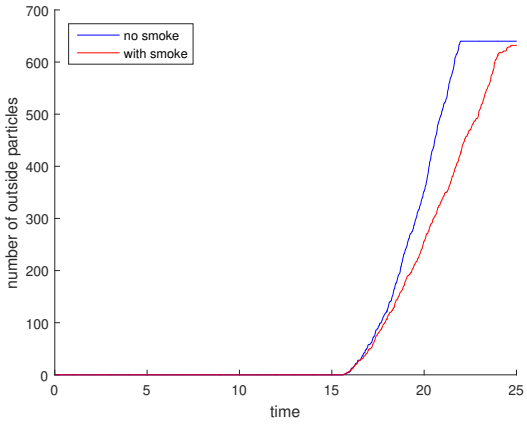
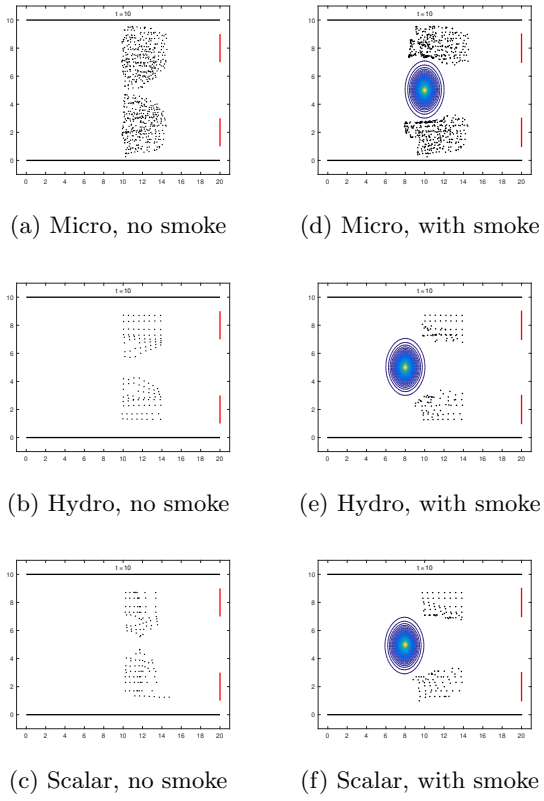


Figure 2: A plot of outside pedestrians of microscopic optimal velocity model ($N_{max} = 5$). The smoke source is at position $(x_s, y_s) = (8, 5)$.



(a) Micro, no smoke (d) Micro, with smoke

(b) Hydro, no smoke (e) Hydro, with smoke

(c) Scalar, no smoke (f) Scalar, with smoke

Figure 3: Distributions of the particles at time $t = 10$ s for scaled microscopic ($N_{max} = 5$), hydrodynamic and scalar models in case with and without smoke.

4.2 Experiment 2

In the second experiment, we perform numerical comparisons between the scaled microscopic optimal velocity model (2.11-2.12), hydrodynamic model (2.20-2.21) and scalar model (2.23) with a source of smoke placed in the middle of corridor. In microscopic simulations, $N_{max} = 1, 3, 5, 10, 20$ are employed to study.

Table 2 shows rum time in hour and number of particles in simulation of scaled microscopic optimal velocity model with smoke source placed in the middle of the corridor. The run time increases as number of particles in microscopic increases. Table 3 demonstrates the rum time in hour and number of particles hydrodynamic and scalar models with smoke source placed in the middle of the corridor. Hydrodynamic model take little longer run time than scalar model. Comparing the run time of microscopic and macroscopic simulations, macroscopic simulations take less time to compute than microscopic simulation when $N_{max} \geq 5$ used in microscopic simulations. This displays the strength of using the macroscopic model over the microscopic model with large number of

N_{max}	Run Time (hour)	#Particles
1	0.3148 h	128
2	0.3212 h	256
3	0.3305 h	384
4	0.3486 h	512
5	0.4928 h	640
10	0.5029 h	1,280
20	1.0675 h	2,560

Table 2: Scaled microscopic model: Maximal particles per cell N_{max}, run time in hour and total number of particles. The smoke source is in the middle of corridor at position (8,5).

Model	Run Time (hour)	#Particles
Hydrodynamic	0.3639 h	200
Scalar	0.3629 h	200

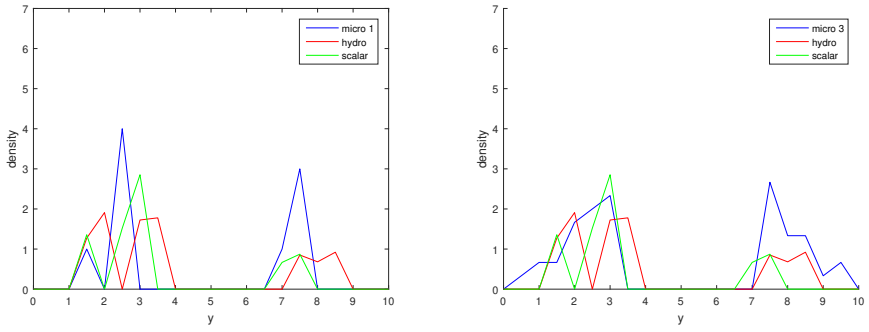
Table 3: Hydrodynamic and scalar models, run time in hour and total number of particles. The smoke source is in the middle of corridor at position (8,5).

particles in simulation.

Figure 4 presents particle density at time $t = 8$ s along the cut $x = 10$ m of the scaled microscopic model with $N_{max} = 1, 3, 5$, hydrodynamic model and scalar model. Figure 5 indicates the comparisons of particle density at time $t = 8$ s along the cut $y = 2$ m of the scaled microscopic model with $N_{max} = 1, 3, 5$, hydrodynamic model and scalar model. Figure 4 and Figure 5 show similar results that particle density of hydrodynamic and scalar models give closed results to scaled microscopic model when $N_{max} = 5$ applied in microscopic simulation. Thus macroscopic models provide a good approximation to scaled microscopic model when number of particles in microscopic simulation is large.

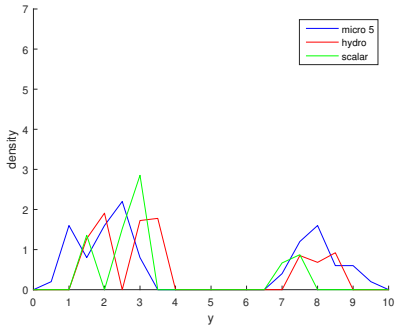
Contour plots for particle density of scaled microscopic, scalar and hydrodynamic models are demonstrated in Figure 6. They give similar results.

The particle distributions at initial time, $t = 5$ s, 10 s and $t = 15$ s of scaled microscopic, scalar and hydrodynamic models are demonstrated in Figure 7. All displays similar results that particles move away from high smoke density areas and move towards the exits.

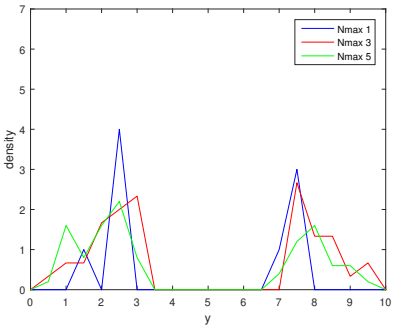


(a) cutx10-comparison

(b) cutx10-comparison

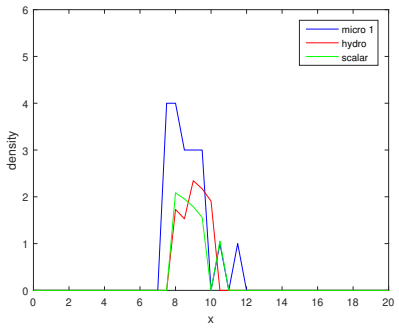


(c) cutx10-comparison

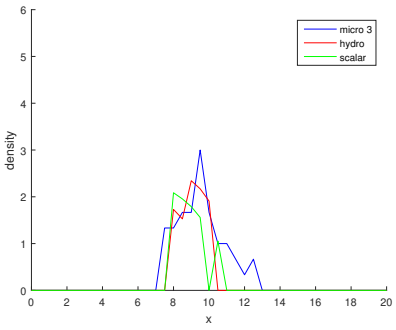


(d) cutx10-microscopic

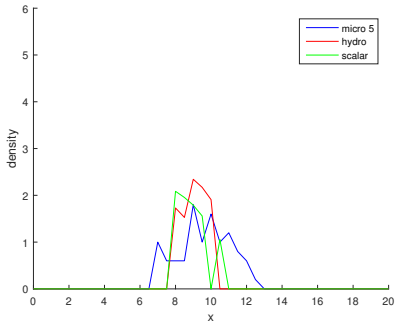
Figure 4: Particle density at $t = 8$ s along $x = 10$ m for scaled microscopic ($N_{max} = 1, 3, 5$), hydrodynamic and scalar models. The smoke source is in the middle of corridor at position $(x_s, y_s) = (8, 5)$.



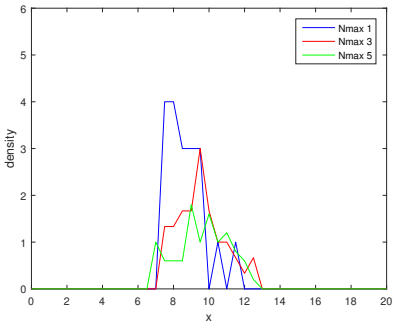
(a) cuty2-comparison



(b) cuty2-comparison

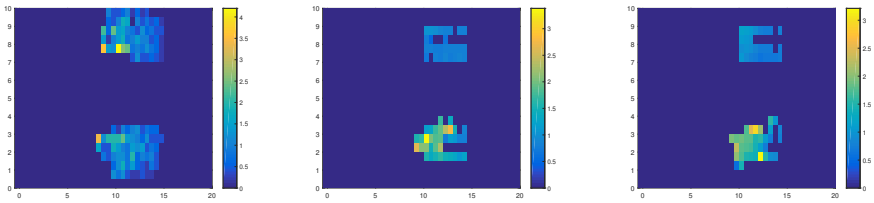


(c) cuty2-comparison



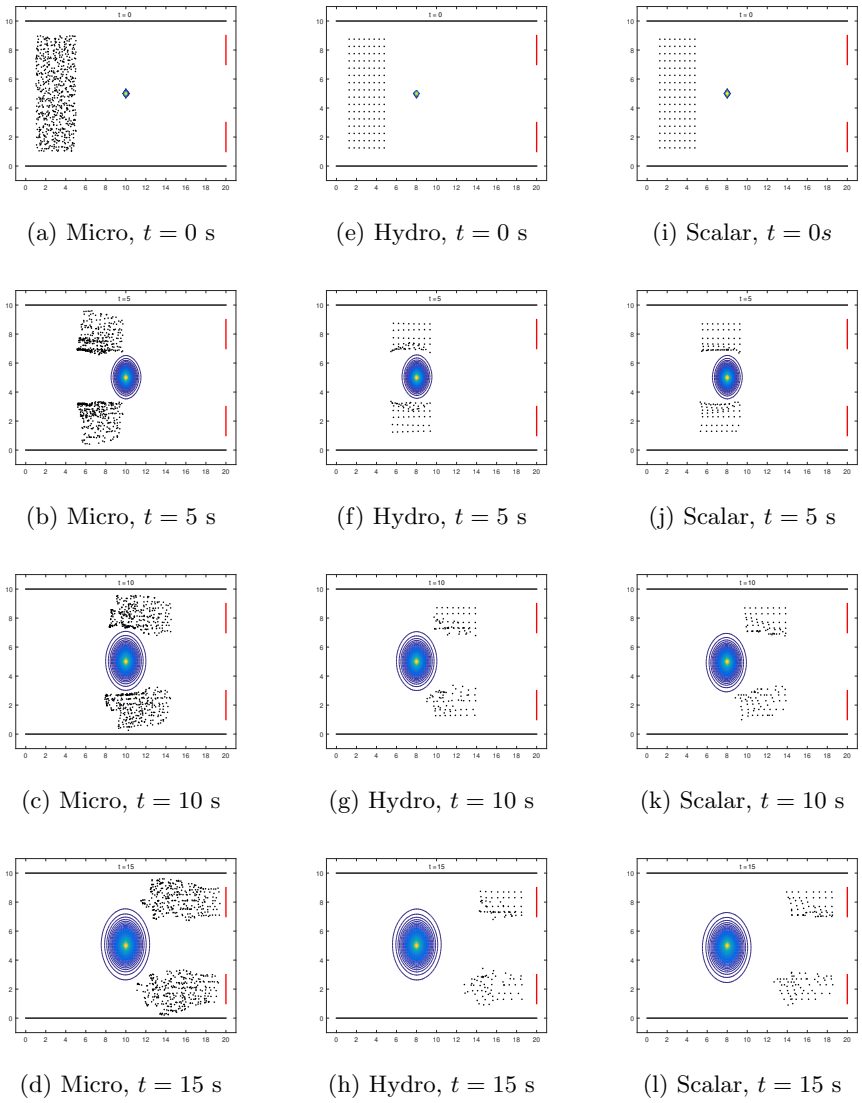
(d) cuty2-microscopic

Figure 5: Particle density at $t = 8s$ along $y = 2m$ for scaled microscopic, hydrodynamic and scalar models. The smoke source is in the middle of corridor at position $(x_s, y_s) = (8, 5)$.



(a) Microscopic (b) Hydrodynamic (c) Scalar

Figure 6: Contour plots of density of scaled microscopic ($N_{max} = 5$), hydrodynamic and scalar models at $t = 10$ s. The smoke source is in the middle of corridor at position $(x_s, y_s) = (8, 5)$.



(a) Micro, $t = 0$ s (e) Hydro, $t = 0$ s (i) Scalar, $t = 0s$

(b) Micro, $t = 5$ s (f) Hydro, $t = 5$ s (j) Scalar, $t = 5$ s

(c) Micro, $t = 10$ s (g) Hydro, $t = 10$ s (k) Scalar, $t = 10$ s

(d) Micro, $t = 15$ s (h) Hydro, $t = 15$ s (l) Scalar, $t = 15$ s

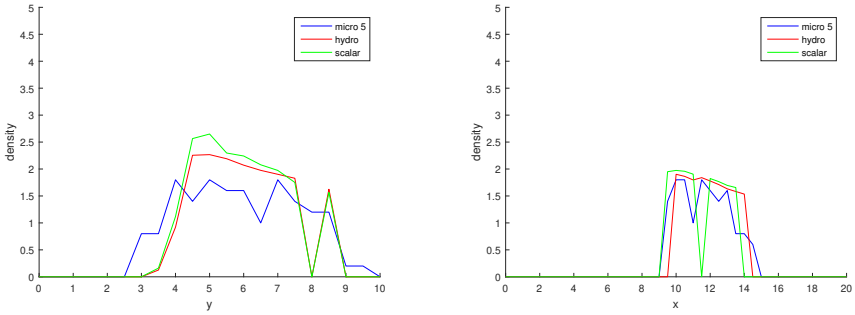
Figure 7: Distributions of particles for scaled microscopic ($N_{max} = 5$), hydrodynamic and scalar models at different times. The smoke source is in the middle of corridor at position $(x_s, y_s) = (8, 5)$.

4.3 Experiment 3

In the third experiment, the scaled microscopic optimal velocity model (2.11-2.12) with $N_{max} = 5$, hydrodynamic model (2.20-2.21) and scalar model (2.23) with a source of smoke placed in front of exit 1 of the corridor, see Figure 10,

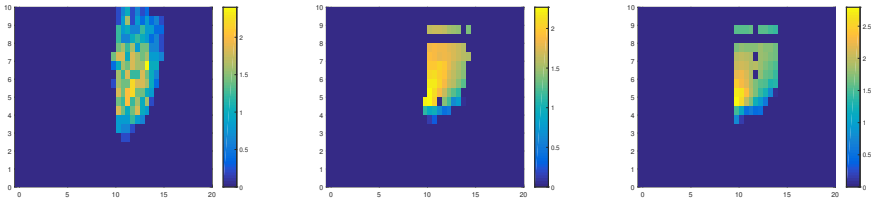
are simulated. We measure particle density at time $t = 10$ s along the cut at $x = 10$ m in Figure 8(a) and along the cut $y = 7$ m in Figure 8(b) for scaled microscopic, hydrodynamic and scalar models. Contour plots of particle density at time $t = 10$ for scaled microscopic, hydrodynamic and scalar models are demonstrated in Figure 9. Particle evolution at initial time, $t = 5$ s, 10 s and 15 s for the third experiment displays in Figure 10. All particles do not move to exit 1 where smoke source is placed. They evacuate out of corridor through exit 2.

Contour plots of arrival time or solution of Eikonal equation (2.5) are demonstrated in Figure 11. Smoke source is in the middle of corridor is shown in Figure 11(a) and smoke source lies in front of exit 1 for Figure 11(b). Large arrival time appears in smoke areas and walls of corridor. Therefore, particles do not move to these areas. Smallest arrival time is raised at the exits, see Figure 11.



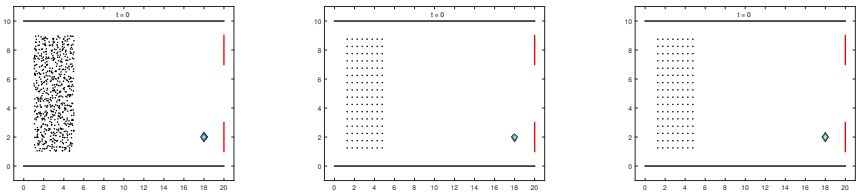
(a) cutx10-comparison (b) cuty7-comparison

Figure 8: Particle density at $t = 10$ s along $x = 10$ m and $y = 7$ m for scaled microscopic, hydrodynamic and scalar model. The smoke source is placed in front of exit 1 at position $(x_s, y_s) = (18, 2)$.

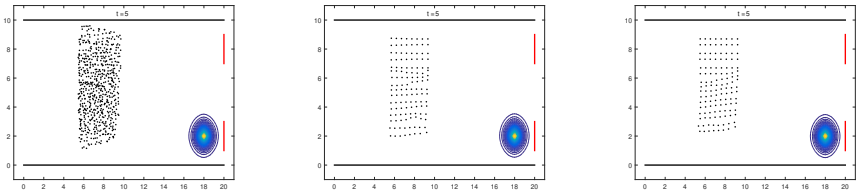


(a) Microscopic (b) Hydrodynamic (c) Scalar

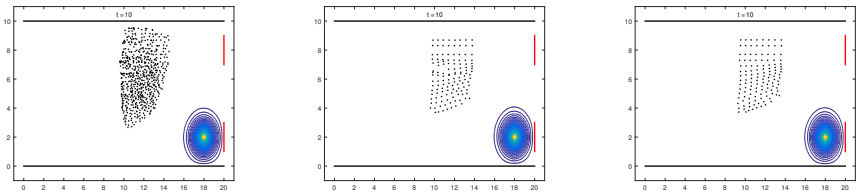
Figure 9: Contour plots of density of scaled microscopic ($N_{max} = 5$), hydrodynamic and scalar models at $t = 10$ s. The smoke source is placed in front of exit 1 at position $(x_s, y_s) = (18, 2)$.



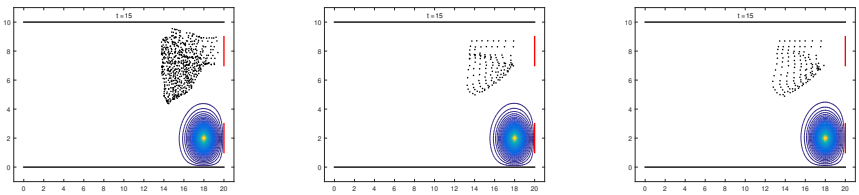
(a) Micro, $t = 0$ s (e) Hydro, $t = 0$ s (i) Scalar, $t = 0$ s



(b) Micro, $t = 5$ s (f) Hydro, $t = 5$ s (j) Scalar, $t = 5$ s

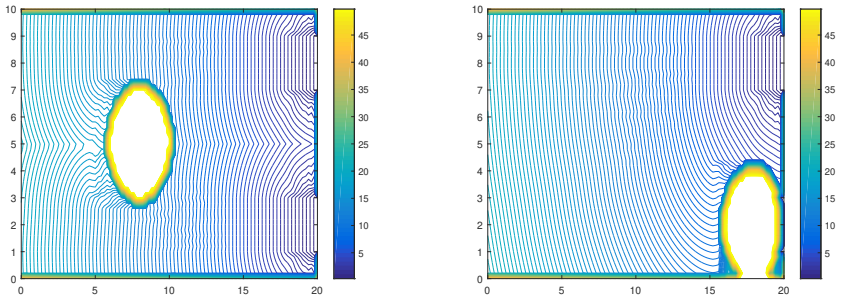


(c) Micro, $t = 10$ s (g) Hydro, $t = 10$ s (k) Scalar, $t = 10$ s



(d) Micro, $t = 15$ s (h) Hydro, $t = 15$ s (l) Scalar, $t = 15$ s

Figure 10: Distributions of particles for scaled microscopic ($N_{max} = 5$), hydrodynamic and scalar models at different times. The smoke source is placed in front of exit 1 at position $(x_s, y_s) = (18, 2)$.



(a) Smoke source is at $(x_s, y_s) = (8, 5)$. (b) Smoke source is in front of exit 1.

Figure 11: Contour plots of solution (estimated arrival time) of the Eikonal equation (2.5) at $t = 10$ s. The source of smoke is lied at position $(x_s, y_s) = (8, 5)$ 11(a) and in front of exit 1 11(b).

5 Conclusions

The proposed microscopic optimal velocity model together with the advection-diffusion equation and the Eikonal equation applied for simulating pedestrians during the dispersion of smoke is presented. The advection-diffusion equation is used for smoke concentration and the Eikonal equation is employed for determining moving directions of particles. The derivations of the corresponding macroscopic models to microscopic optimal velocity model are demonstrated. Numerical experiments on the microscopic optimal velocity model are performed in the case with and without smoke. Results show that pedestrians take longer time to evacuate in presence of smoke compared to the case without smoke. Then experiments on the scaled microscopic optimal velocity model, the corresponding hydrodynamic and scalar models are executed on the domain with smoke and the comparisons of results are shown. The scaled microscopic optimal velocity model provides a good estimate to macroscopic models when large number of particles are adopted in microscopic simulations. When $N_{max} \geq 5$ is used in each cell of microscopic model, it takes longer time to compute compared to macroscopic models. This outcome shows the advantage of using macroscopic models over the microscopic model. In situations where there are many particles in simulation, macroscopic models would be an appropriate choice to employ for study since it takes less computation time than microscopic model. Clogging or arching effect around the exits, which is natural phenomena usually occurred in crowds, are observed in our models.

Credit authorship contribution statement

J. Makmul contributes conception and design of the work, performs formal analysis and writes the manuscript.

Declaration of competing interest

The author(s) declare that they have no conflicts of interest.

Data availability

No data was used for the research described in the article.

Acknowledgments

The author is very grateful for the working environments provided by the Department of Mathematics, Science Faculty at the Kasetsart University, Thailand.

References

[1] J. Makmul, A cellular automaton model for pedestrians' movements influenced by gaseous hazardous material spreading, *Modelling and Simulation in Engineering*, (2020), pp. 1–10.

[2] D. Helbing, L. Buzna, A. Johansson, T. Werner, Self-organized pedestrian crowd dynamics: Experiments, simulations, and design solutions, *Transportation Science*, (2005), pp. 1–24.

[3] J. Makmul, A pedestrian evacuation model with leaders during the smoke dispersion based on a social force model, *Modelling and Simulation in Engineering*, (2023), pp. 1–21.

[4] J. Makmul, A hierarchy of the optimal velocity model with optimal path for pedestrian evacuation: From microscopic to macroscopic models, *Physica A: Statistical Mechanics and its Applications*, (2024), pp. 1–13.

[5] S. Okazaki, A study of simulation model for pedestrian movement with evacuation and queuing, Part 1: Pedestrian Movement by the Application on of Magnetic Models. *Trans. of A.I.J.*, 35(283), (1979), pp. 111–119.

[6] G. Antonini, M. Bierlaire, M. Weber, Discrete choice models of pedestrian walking behavior, *Transportation Research Part B 40*, (2006), pp. 667–687.

[7] C. Dogbe, On the modelling of crowd dynamics by generalized kinetic models, *J. Math. Anal. Appl. 387*, (2012), pp. 512–532.

[8] V. Coscia, C. Canavesio, First-order macroscopic modelling of human crowd dynamics, *Math. Mod. Meth. Appl. Sci. 18*, (2008), pp. 1217–1247.

[9] R. Etikyala, S. Goettlich, A. Klar, S. Tiwari, A macroscopic model for pedestrian flow: Comparisons with experiment results of pedestrian flow in corridors and T-junctions, *Neural, Parallel, and Scientific Computations*, (2014), pp. 315–330.

[10] A. Nakayama, Y. Sugiyama, Two-dimensional optimal velocity model for pedestrians and biological motion, *AIP Conference Proceedings*, 661(1), (2003), p. 107.

[11] J. Makmul, A pedestrians flow model during propagation of smoke: Microscopic and macroscopic approaches, *Safety Science*, (2021), pp. 1–11.

[12] J. Sethian, Fast marching methods and level set methods for propagating interfaces, University of California, Berkeley 94720, (1998).

[13] S. Göttlich, A. Klar, E. Ragavendar, S. Tiwari, Particle methods for pedestrian flow models: from microscopic to non-local continuum models., *Math. Models Methods Appl. Sci. 24*, 2503, (2014).

[14] J. Carrillo, M. D'Orsogna, V. Panferov, Double milling in self-propelled swarms from kinetic theory, *Kinetic and related models 2*, (2009), pp. 363–378.

[15] S. Göttlich, Complex material flow problems: a multi-scale model hierarchy and particle methods, Engineering Mathematics, 92(1), (2015), pp. 15–29.

[16] S. Cao, W. Song, X. Liu, N. Mu, Simulation of pedestrian evacuation in a room under fire emergency, Procedia Engineering 71. *Elsevier Ltd.*, (2014), pp. 403–409.

[17] G. Mulholland, Smoke production and properties, *The SFPE Handbook of Fire Protection Engineering*, second ed., (1995), pp. 217–227.

[18] Y. Chuang, M. D'Orsogna, D. Marthaler, A. Bertozzi, L. Chayes, State transitions and the continuum limit for a 2D interacting, self-propelled particle system, *Physica D 232*, (2007), pp. 33–47.

[19] J. Chen, J. Beraun, T. Carney, A corrective smoothed particle method for boundary value problems in heat conduction, *Internat. J. Numerical Methods in Engineering 46*, (1999), pp. 231–252.

[20] M. Liu, G. Liu, Restoring particle consistency in smoothed particle hydrodynamics, *Applied numerical mathematics 56*, (2006), pp. 19–36.